7-6-2006

Non-Destructive Recovery of Voids within a Three Dimensional Domain Using Thermal Imaging

Victor B. Oyeyemi

NON-DESTRUCTIVE RECOVERY OF VOIDS WITHIN A THREE DIMENSIONAL DOMAIN USING THERMAL IMAGING

Victor B. Oyeyemi
Advisor: Kurt Bryan

MS TR 06-01

July 6, 2006

Department of Mathematics
Rose-Hulman Institute of Technology

FAX : (812) 877-8883 **Phone: (812) 877-8391**

Non-Destructive Recovery of Voids within a Three Dimensional Domain using Thermal Imaging

Victor B. Oyeyemi

6 July 2006

Abstract

We develop an algorithm capable of detecting the presence of spherical voids in a thermally conducting object. In addition, the process recovers both the radii and locations of each void. Our method involves the application of a known steady-state heat flux to the object's boundary and measurement of the induced steady-state temperature on the boundary.

Contents

1 Introduction

The problem of imaging defects in objects is of industrial importance. This task is often complicated by the need to image the defects without destroying the object. One way of doing this is X-ray imaging. However, this method may not be suited to every application. Thermal imaging and impedance imaging – the use of electrical current – are other methods currently being investigated in numerous areas. See [3] .

In this paper we develop an algorithm for imaging defects that are in the shape of spherical voids within an arbitrary three-dimensional domain. We assume the object is thermally conducting, homogeneous, with an interior that is inaccessible. We apply a known heat flux to the object's boundary and solve the inverse problem of recovering the void(s) from the induced boundary temperature measurements. The inverse problem is solved by employing the Reciprocity Gap [1] approach.

Other groups have worked on different versions of this problem, e.g., [5, 6]. For example, Talbott and Spring [6] studied the recovery of voids within a two dimensional domain. This work is mainly an extension to three dimensions of these previous projects.

In the next section we give a description of the forward problem. This is followed in Section 3 by the formulation of the inverse problem. Also in Section 3, we give a proof to a uniqueness theorem which shows that voids can be uniquely recovered from thermal data. Sections 4 and 5 are devoted to formulating the Reciprocity gap functional and test functions. In Section 6, we work on recovering a single void, and in Section 7, multiple voids. In both of Sections 6 and 7, we include numerical examples to show the effectiveness of our algorithm.

2 Forward Problem

Consider a three-dimensional domain Ω with a single internal void D. The steady-state temperature anywhere in Ω can be determined, in theory, if we know the shape, size, location, and the thermal properties (including the boundary and initial conditions) of Ω, as well as that of the void D. Let us denote the boundary of Ω as $\partial\Omega$ and that of the void as ∂D. Assume a steady heat flux g is applied to $\partial\Omega$ and that the boundary of the void D is perfectly insulating. The equations governing the steady-state behavior of the system are

$$\Delta u = 0 \text{ in } \Omega/D, \tag{1}$$

$$\frac{\partial u}{\partial \mathbf{n}} = g \text{ on } \partial\Omega, \tag{2}$$

$$\frac{\partial u}{\partial \mathbf{n}} = 0 \text{ on } \partial D \tag{3}$$

In the equations above, $u(x, y, z)$ denotes the temperature at point (x, y, z) in $\Omega \setminus D$ and Δu is the Laplacian of the temperature. In cartesian co-ordinate, $\Delta u = \frac{\partial^2 u}{\partial x^2} + \frac{\partial^2 u}{\partial y^2} + \frac{\partial^2 u}{\partial x^2}$. The expression $\partial u/\partial \mathbf{n} := \nabla u \cdot \mathbf{n}$ is the heat flux in the direction of the outward unit normal $\mathbf{n}$ on $\partial\Omega$ or ∂D, as appropriate. In order for equations (1)-(3) to possess a solution, it is necessary that $\int_{\partial\Omega} g dS = 0$, which means physically that the net heat flux going into Ω equals zero. Moreover, the solution to equations (1)-(3) is unique only up to an additive constant. A unique solution can be obtained by imposing an additional normalizing condition, e.g.,

$$\int_{\partial\Omega} u \, dS = 0$$

where dS denotes surface measure. See Figure 1 below.

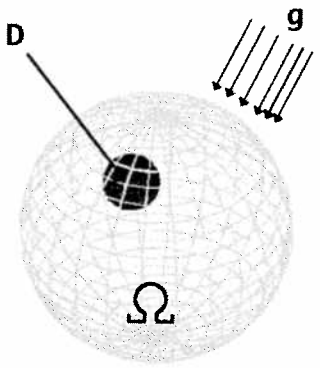

Figure 1: A region Ω with Spherical Void D

As we mentioned earlier, if the size, shape, and location of the void are known, we can write out the solution to the equations above, at least up to an additive constant. This is the so-called *forward problem*: we have a partial differential equation on a given region (the domain Ω minus the void(s)) and the goal is to obtain the solution, that is, the temperature of the region. In the next section we formulate the *inverse problem*, which describes the situation when we know something about the temperature in all or part of the system and we want to use this knowledge to obtain information on the voids.

3 Inverse Problem

Suppose we pump in a steady flux g into $\partial\Omega$ and then measure the induced temperature u on $\partial\Omega$. Remember that the object we are working with is internally inaccessible, so the boundary temperature is all we have. From the boundary temperature data and the flux

that produced it, we hope to image the internal void as accurately as possible. The function u is of course governed by equations (1) - (3). However, we are now solving for the geometry of the void D, instead of the temperature u.

A standard argument commonly used in the field of inverse problems and given below shows that any void can be uniquely recovered from one such input flux/temperature measurement, provided the input flux is not identically zero. This proof is based on the following two "Unique Continuation" theorems [4] which we state here without proof:

Theorem 1: Let u_1 and u_2 be harmonic functions in a connected domain B, and suppose that u_1 and u_2 agree on some open ball contained in B. Then $u_1 \equiv u_2$ throughout B.

Theorem 2: Let u_1 and u_2 be harmonic functions in a connected domain B, and suppose that $u_1 = u_2$ and $\frac{\partial u_1}{\partial \mathbf{n}} = \frac{\partial u_2}{\partial \mathbf{n}}$ on some open portion of ∂B. Then $u_1 \equiv u_2$ throughout B.

We now make use of the above two theorems to give a proof that the inverse problem has a unique solution [4]:

Uniqueness Theorem: Let D_1 and D_2 be two voids in Ω, and let $\Omega_k = \Omega / D_k$ for $k = 1, 2$. Suppose u_1 and u_2 are harmonic on Ω_1 and Ω_2, respectively, with $\frac{\partial u_k}{\partial \mathbf{n}} = g$ on $\partial\Omega$ for $k = 1, 2$, and $\frac{\partial u_k}{\partial \mathbf{n}} = 0$ on ∂D_k for $k = 1, 2$. Assume g is not identically zero. If $u_1 = u_2$ on any open portion of $\partial\Omega$ then $D_1 = D_2$.

Proof: The functions u_1 and u_2 are both harmonic on $\Omega/(D_1 \cup D_2)$. Since they have the same Cauchy data (the Cauchy data means the value of the function AND its normal derivative) on some open portion of $\partial\Omega$, we have by Theorem 2 that $u_1 \equiv u_2$ throughout $\Omega/(D_1 \cup D_2)$.

We can derive a contradiction by supposing that $D_1 \neq D_2$; in this case at least one of D_2/D_1 or D_1/D_2 is non-empty, so we'll assume the former. Let $E = D_2/D_1$. In this case we find that u_1 is defined on E, and moreover, $\frac{\partial u_1}{\partial \mathbf{n}} \equiv 0$ on E. This means that u_1 must be constant on E, because from the Divergence Theorem we have

$$0 = \int_{\partial E} u_1 \frac{\partial u_1}{\partial \mathbf{n}} \, dS = \int_E \nabla \cdot (u_1 \nabla u_1) \, dV = \int_E (u_1 \triangle u_1 + \nabla u_1 \cdot \nabla u_1) \, dV = \int_E |\nabla u_1|^2 dV$$

since $\triangle u_1 = 0$ and $\nabla u_1 \cdot \nabla u_1 = |\nabla u_1|^2$. From $\int_E |\nabla u_1|^2 dV = 0$ we must conclude that $\nabla u_1 \equiv 0$ (since the integrand is non-negative) and hence u_1 is constant in E. It doesn't matter what the constant is.

Since u_1 (defined on Ω/D_1) agrees with a constant function (which is harmonic), the function u_1 is constant throughout Ω/D_1, which forces $g = \frac{\partial u_1}{\partial n} = 0$, a contradiction. We

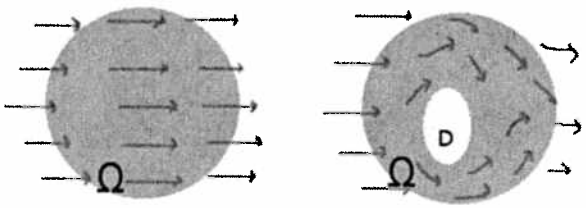

Figure 2: Effect of void on heat flow

therefore conclude that $D_1 \neq D_2$, which completes the proof.

Figure 2 provides an intuitive picture that illustrates why we can recover the domain D. The figure contains two similar domains, Ω and $\Omega \setminus D$. If we apply the same heat flux to both domains, we see that the heat sails through the left one, Ω, unimpeded, while the defect causes a slight perturbation in the heat flow in the domain $\Omega \setminus D$. Thus we expect a difference in the boundary temperature of the two domains. In fact, we expect different defects to produce slightly different perturbation signatures (as we have shown in the Uniqueness Theorem above). The difficulty is to find method for actually reconstructing D explicitly and efficiently.

4 The Reciprocity Gap Approach

4.1 The Reciprocity Gap Formula

In order to solve the inverse problem, we will employ what is called the Reciprocity Gap functional [1]. Let us outline the derivation of this functional from Green's second identity. Recall that Green's second identity states that for any pair of functions f and w contained in $C^2(\overline{B})$ for a bounded domain B we have

$$\int\int_B (f\Delta w - w\Delta f)\, dA = \int_{\partial B} \left(f\frac{\partial w}{\partial \mathbf{n}} - w\frac{\partial f}{\partial \mathbf{n}} \right)\, dS$$

Let $B = \Omega \setminus D$, take $f = u$ on $\Omega \setminus D$, and let w be a known function which is harmonic on all of Ω (hence on $\Omega \setminus D$) to obtain

$$0 = \int\int_{\Omega/D} (u\Delta w - w\Delta u) dA \;\; = \;\; \int_{\partial\Omega \cup \partial D} \left(u\frac{\partial w}{\partial \mathbf{n}} - w\frac{\partial u}{\partial \mathbf{n}} \right)\, dS$$

$$= \int_{\partial\Omega} \left(u\frac{\partial w}{\partial \mathbf{n}} - w\frac{\partial u}{\partial \mathbf{n}} \right) dS - \int_{\partial D} \left(u\frac{\partial w}{\partial \mathbf{n}} - w\frac{\partial u}{\partial \mathbf{n}} \right) dS. \quad (4)$$

In the above we are taking (for later convenience) the normal $\mathbf{n}$ on ∂D to point OUT of D, hence into $\Omega \setminus D$. The negative sign appears in the left side of the last equation because the outward normal to $\partial\Omega \cup \partial D$ is the negative of the outward normal to ∂D. With equations (2) and (3) in equation (4) we can write

$$RG(w) := \int_{\partial\Omega} \left(u\frac{\partial w}{\partial \mathbf{n}} - wg \right) dS = \int_{\partial D} u\frac{\partial w}{\partial \mathbf{n}} \, dS \quad (5)$$

It is important to note that we can compute the reciprocity gap functional $RG(w)$ for any chosen harmonic function w, since we know g and u on $\partial\Omega$. We thus have the ability to compute the integral on the right in equation (5). With the use of special choices for the test function w, we will be able to exploit this ability to recover information about D.

4.2 Test Functions

The test function w in the reciprocity gap function must be harmonic in Ω. At this point, we pick a class of test functions that satisfies this condition and use these functions to obtain the center and radius of the defect. The class of test functions we consider are those of the form

$$w = Ce^{p_x x + p_y y + p_z z}$$

for complex numbers C, p_x, p_y, p_z. That w be harmonic forces $p_x^2 + p_y^2 + p_z^2 = 0$. This is easily seen from taking the Laplacian of w:

$$\begin{aligned} \Delta w &= \frac{\partial^2 w}{\partial x^2} + \frac{\partial^2 w}{\partial y^2} + \frac{\partial^2 w}{\partial x^2} \\ &= p_x^2 w + p_y^2 w + p_z^2 w \end{aligned}$$

Therefore, $\Delta w = 0$ implies $p_x^2 + p_y^2 + p_z^2 = 0$, since w is nonzero.

If we choose p_x to be zero then we must have $p_z = \pm i p_y$. Let us take $p_y = p$ for some p and $p_z = ip$. We also set $C = 1/p$ (with the restriction that $p \neq 0$). We obtain a sub-class of harmonic test functions

$$w_p^1(x, y, z) = \frac{e^{py + ipz}}{p}. \quad (6)$$

Similarly, if we set p_y to zero we can construct a second sub-class of test functions

$$w_p^2(x,y,z) = \frac{e^{px+ipz}}{p}. \tag{7}$$

We will also need $\partial w_p^1/\partial \mathbf{n}$ and $\partial w_p^2/\partial \mathbf{n}$. We find that

$$\begin{aligned} \frac{\partial w_p^1}{\partial \mathbf{n}} &= \nabla w_p^1 \cdot \mathbf{n} \\ &= e^{py+ipz} < 0, 1, i > \cdot \mathbf{n} \end{aligned}$$

and

$$\begin{aligned} \frac{\partial w_p^2}{\partial \mathbf{n}} &= \nabla w_p^2 \cdot \mathbf{n} \\ &= e^{px+ipz} < 1, 0, i > \cdot \mathbf{n} \end{aligned}$$

As we will see in the next section, these two sub-classes of test functions will allow us to easily obtain the center of the void.

5 Imaging a Single Void

In this section we will work on imaging a single void. In the next section we will extend the results for one void to the case where we have multiple voids.

We now define the problem geometrically. We assume D is spherical with center (a,b,c) and radius R. The surface ∂D of the void can be parameterized as

$$\begin{aligned} x &= a + R\sin\varphi\cos\theta \\ y &= b + R\sin\varphi\sin\theta \qquad 0 \le \varphi \le \pi \\ z &= c + R\cos\varphi \qquad\quad 0 \le \theta \le 2\pi \end{aligned}$$

With this parameterization we find that surface measure is given by $ds = \sin(\varphi)\, d\varphi\, d\theta$.

For $(x,y,z) \in \partial D$ equation (6) can be written as

$$\begin{aligned} w_p^1 &= \frac{1}{p} e^{p(b+R\sin\varphi\sin\theta+ic+iR\cos\varphi)} \\ &= \frac{1}{p} e^{p(b+ic)} e^{pR(\sin\varphi\sin\theta+iR\cos\varphi)} \\ &\approx \frac{e^{p(b+ic)}}{p} \end{aligned} \tag{8}$$

where we have assumed R is small and used the approximation

$$e^{pR(\sin\varphi\sin\theta+i\cos\varphi)} = 1 + O(R)$$

Similarly, for small R we approximate equation (7) as

$$w_p^2 \approx \frac{e^{p(a+ic)}}{p}. \tag{9}$$

Note that the outward unit normal vector on ∂D with our parameterization is given by

$$\mathbf{n} =< \sin\varphi\cos\theta,\ \sin\varphi\sin\theta,\ \cos\varphi > \tag{10}$$

5.1 Finding The Center of a Single Void

Use of the approximations to the test functions from (8) and (9) in the gap reciprocity function (5) yields

$$\begin{aligned} RG(w_p^1) &= \int_0^{2\pi}\int_0^{\pi} u\frac{\partial w_p^1}{\partial n}\, R^2\sin\varphi d\theta d\varphi \\ &= \int_0^{2\pi}\int_0^{\pi} ue^{py+ipz} < 0,1,i > \cdot\mathbf{n}\, R^2\sin\varphi d\theta d\varphi \\ &\approx e^{p(b+ic)}\int_0^{2\pi}\int_0^{\pi} u < 0,1,i > \cdot\mathbf{n}\, R^2\sin\varphi d\theta d\varphi \end{aligned} \tag{11}$$

and

$$\begin{aligned} RG(w_p^2) &= \int_0^{2\pi}\int_0^{\pi} u\frac{\partial w_p^2}{\partial n}\, R^2\sin\varphi d\theta d\varphi \\ &= \int_0^{2\pi}\int_0^{\pi} ue^{px+ipz} < 1,0,i > \cdot\mathbf{n}\, R^2\sin\varphi d\theta d\varphi \\ &\approx e^{p(a+ic)}\int_0^{2\pi}\int_0^{\pi} u < 1,0,i > \cdot\mathbf{n}\, R^2\sin\varphi d\theta d\varphi \end{aligned} \tag{12}$$

The functions $\frac{\partial w_p^1}{\partial p}$ and $\frac{\partial w_p^2}{\partial p}$ are also harmonic (as functions of x, y, and z). Use of these as test functions in the reciprocity gap functional, with similar approximations to those above, yields

$$RG(\partial w_p^1/\partial p) = (b+ic)e^{p(b+ic)}\int_0^{2\pi}\int_0^{\pi} u < 0,1,i > \cdot\mathbf{n}\, R^2\sin\varphi d\theta d\varphi \tag{13}$$

and

$$RG(\partial w_p^2/\partial p) \;=\; (a+ic)e^{p(a+ic)}\int_0^{2\pi}\int_0^{\pi} u < 1,0,i > \cdot \mathbf{n}\, R^2 \sin\varphi d\theta d\varphi \tag{14}$$

If we combine equations (13) and (11) we have

$$\frac{RG(\partial w_p^1/\partial p)}{RG(w_p^1)} \;\approx\; (b+ic) \tag{15}$$

while equations (14) and (12) yield

$$\frac{RG(\partial w_p^2/\partial p)}{RG(w_p^2)} \;\approx\; (a+ic) \tag{16}$$

from which we can recover a, b, and c, by numerically computing the left hand sides of the equations.

5.2 Recovering the Radius

To find the radius of the void, we use $RG(w)$, which we restate here for convenience:

$$RG(w) = \int_{\partial D} u\frac{\partial w}{\partial \mathbf{n}}\, dS$$

The main goal in this section will be to (partially) prove the following theorem:

Theorem 4: For any harmonic function $w = e^{p_x x + p_y y + p_z z}$ we have

$$RG(w) = 2\pi R^3 \nabla u_0(a,b,c)\cdot q e^{q\cdot r} + O(R^4)$$

where $q =< p_x, p_y, p_z >$ and $d = (a,b,c)$ is the center of a void of radius R and u_0 is the harmonic function on Ω with Neumann data g.

We now prove this theorem, but omit a certain technical portion which can be shown using methods similar to those of [2]

Proof of Theorem 4: Let us write $u = u(r,\varphi,\theta)$ with $r \geq R$ to denote u on or outside the surface of the void D of radius $r = R$, with (r,φ,θ) denoting spherical coordinates about the center (a,b,c) of D as before. We would like to obtain an explicit but good approximation for u.

Take u_0 to be the solution to the heat equation if no void were present in Ω. If we define a quantity v as $v = u - u_0$, then using the fact that $\Delta u_0 = 0$ and equations (1) - (3) on page

3 shows that v satisfies

$$\Delta v = 0 \text{ in } \Omega/D \tag{17}$$

$$\frac{\partial v}{\partial \mathbf{n}} = 0 \text{ on } \partial\Omega \tag{18}$$

$$\frac{\partial v}{\partial \mathbf{n}} = -\frac{\partial u_0}{\partial \mathbf{n}} \text{ on } \partial D \tag{19}$$

We will ignore the condition (18), and instead seek a solution which rapidly decays with respect to r as $r \to \infty$. The techniques of [2] can be adapted to this setting to show that this introduces an error of order $O(R^4)$ to our final approximation.

It is worth noting that on ∂D we have $\frac{\partial}{\partial \mathbf{n}} = \frac{\partial}{\partial r}$. As a consequence we have

$$\begin{aligned}
\frac{\partial u_0}{\partial \mathbf{n}} &= \nabla u_0 \cdot \mathbf{n} \\
&= \nabla u_0(a + R\sin\varphi\cos\theta, c + R\sin\varphi\sin\theta, c + R\cos\varphi) \cdot < \sin\varphi\cos\theta,\ \sin\varphi\sin\theta,\ \cos\varphi > \\
&= \nabla u_0(a, b, c) \cdot < \sin\varphi\cos\theta,\ \sin\varphi\sin\theta,\ \cos\varphi > + O(R)
\end{aligned}$$

for small R, where we have made use of equation (10) and the fact that

$$\nabla u_0(a + R\sin\varphi\cos\theta, c + R\sin\varphi\sin\theta, c + R\cos\varphi) = \nabla u_0(a, b, c) + O(R).$$

Thus from equation (19) we find

$$\frac{\partial v}{\partial r} = \frac{\partial v}{\partial \mathbf{n}} = -\nabla u_0(a, b, c) \cdot < \sin\varphi\cos\theta,\ \sin\varphi\sin\theta,\ \cos\varphi > + O(R). \tag{20}$$

A straightforward separation of variables argument shows that the harmonic function $v(r, \varphi, \theta)$ which satisfies (20) and decays at infinity is given by

$$v(r, \varphi, \theta) = R^3 \frac{\nabla u_0(a, b, c) \cdot < \sin\varphi\cos\theta,\ \sin\varphi\sin\theta,\ \cos\varphi >}{2r^2}$$

and on $r = R$ this is

$$v \approx R\frac{\nabla u_0(a, b, c) \cdot < \sin\varphi\cos\theta,\ \sin\varphi\sin\theta,\ \cos\varphi >}{2} \tag{21}$$

This approximation for v uniquely satisfies (17) and (19) while condition (18) is ignored. Instead, we have $\frac{\partial v}{\partial \mathbf{n}}$ on $\partial\Omega$ decaying very fast as r goes to infinity.

A straightforward linearization of $u_0(x,y,z)$ for $(x,y,z) \in D$ yields

$$u_0 = u_0(a,b,c) + R\nabla u_0(a,b,c)\cdot < \sin\varphi\cos\theta,\ \sin\varphi\sin\theta,\ \cos\varphi > +O(R^2).$$

Using this approximation and that for v, we obtain, to order $O(R^2)$,

$$\begin{aligned} u &= u_0 + v \\ u &\approx u_0(a,b,c) + \frac{3}{2}R\nabla u_0(a,b,c)\cdot < \sin\varphi\cos\theta,\ \sin\varphi\sin\theta,\ \cos\varphi > \end{aligned} \tag{22}$$

In what follows, we use this approximation for u in the reciprocity gap functional and simplify. First, define vectors $d =< a,b,c >$ and $q =< p_x,p_y,p_z >$. Our class of test functions has the form $w = e^{d\cdot q}$ and $\frac{\partial w_p}{\partial n} = (q\cdot\mathbf{n})e^{q\cdot d}$. Note that we have dropped the terms containing R which we still assume is small. So, we have

$$\begin{aligned} RG(w_p) &= \int_0^{2\pi}\int_0^{\pi}(u_0(a,b,c) + \frac{3}{2}R\nabla u_0(a,b,c)\cdot\mathbf{n})(q\cdot\mathbf{n})e^{q\cdot d}\,R^2\sin\varphi d\theta d\varphi \\ &= R^2e^{q\cdot r}\int_0^{2\pi}\int_0^{\pi}u_0(a,b,c)(q\cdot\mathbf{n})\sin\varphi d\theta d\varphi \\ &+ \frac{3}{2}R^3e^{q\cdot d}\int_0^{2\pi}\int_0^{\pi}\nabla u_0(a,b,c)\cdot\mathbf{n}(q\cdot\mathbf{n})\ \sin\varphi d\theta d\varphi \\ &= \frac{3}{2}R^3e^{q\cdot r}\int_0^{2\pi}\int_0^{\pi}\nabla u_0(a,b,c)\cdot\mathbf{n}(q\cdot\mathbf{n})\ \sin\varphi d\theta d\varphi \\ &= \frac{3}{2}R^3e^{q\cdot r}\cdot\frac{4}{3}\pi\nabla u_0(a,b,c)\cdot q \\ &= 2\pi R^3\nabla u_0(a,b,c)\cdot qe^{q\cdot d} \end{aligned} \tag{23}$$

where we have made use of (10). This final equation completes the proof of Theorem 4.

We now have a method for recovering R, for we can compute $RG(w)$ on the right in Theorem 4 from boundary data, while on the left we know all quantities except R (if we've recovered the center already).

5.3 Numerical Test

Indeed, the formulas (15) , (16), and (23) are very effective in imaging voids. We were able to image several voids within a spherical domain. The results can be better illustrated with a specific example.

We used Femlab to construct a domain Ω which is a unit sphere centered at the origin. We then carved out a spherical void D of radius 0.2, centered at $(0.2, 0.1, 0.5)$. We simulated

the solution to the system using the heat flux $g = \sin\varphi$ (in spherical coordinates, or $g = z$ in rectangular). This Femlab solution provided us with temperature data on various points on the boundary of Ω, at 50 uniformly separated longitudinal and 25 uniformly separated latitudinal points on Ω. Also, it can be easily verified that with our choice of g, the temperature if no void were present in Ω is $u_0(x, y, z) = z$.

Using an algorithm written in Maple we computed the RG function and it's derivatives with respect to p. From these, we were able to recover a void with center $(0.199, 0.090, 0.504)$ and radius (0.201). This result is clearly a good one as it agrees quite well with the actual void—see the figure below. This result was obtained with a p value of 0.2. Theoretically, the recovery should be successful independent of the p values used. However, we obtained variations ranging from very minute to significant for different values of p. This discrepancies are due to numerical instabilities in the algorithm used.

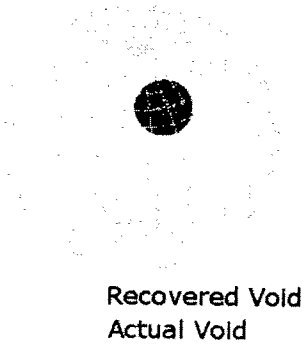

Figure 3: Actual and Recovered Void

6 Imaging Multiple Voids

What we have done so far can be easily extended to cases where we have multiple voids [3]. Assume there are N non-overlapping voids D_i, for $i = 1..N$, within Ω. Let the center and radius of void D_i be R_i and (a_i, b_i, c_i), respectively. In this case, the Gap Reciprocity functional has the form

$$RG(w) := \int_{\partial\Omega} \left(u\frac{\partial w}{\partial \mathbf{n}} - w\frac{\partial u}{\partial \mathbf{n}} \right) dS = \sum_{i=1}^{N} \int_{\partial D_i} u\frac{\partial w}{\partial \mathbf{n}} dS \tag{24}$$

6.1 Finding The Center of Each Void

With test function $w = w_p^1 = e^{py+ipz}$ let us define $\phi_1(p) := RG(w_p^1)$, and similar set $\phi_2(p) := RG(w_p^2)$, where $w_p^2 = e^{px+ipz}$. A similar argument to that in the single void case yields

$$\phi_1(p) = \sum_{i=1}^{N} e^{pz_i^1} \int_0^{2\pi} \int_0^{\pi} u_i(\varphi,\theta) < 1,0,i > \cdot \mathbf{n}\, R^2 \sin\varphi d\theta d\varphi \tag{25}$$

and

$$\phi_2(p) = \sum_{i=1}^{N} e^{pz_i^2} \int_0^{2\pi} \int_0^{\pi} u_i(\varphi,\theta) < 1,0,i > \cdot \mathbf{n}\, R^2 \sin\varphi d\theta d\varphi \tag{26}$$

where $z_i^1 = b_i + ic_i$ and $z_i^2 = a_i + ic_i$. Here we use $u_i(\varphi,\theta)$ to denote the restriction of u to ∂D_i, again in spherical coordinates based at the center of D_i.

For simplicity we rewrite (25) and (26) as $\phi_1(p) = \sum_{i=1}^{N} e^{pz_i^1} J_i^1$ and $\phi_2(p) = \sum_{i=1}^{N} e^{pz_i^2} J_i^2$, in which J_i^1 and J_i^2 are, respectively the integral terms in (25) and (26). They are constants in p.

Because each of the functions $\phi_1(p)$ and $\phi_2(p)$ is a sum of simple exponentials in p, each must satisfy an ordinary differential equations (ODE) of the form

$$c_N \phi_1^{(N)}(p) + c_{N-1}\phi_1^{(N-1)}(p) + c_{N-2}\phi_1^{(N-2)}(p) + \ldots + c_1\phi_1'(p) + c_0\phi_1(p) = 0 \tag{27}$$

or

$$d_N \phi_2^{(N)}(p) + d_{N-1}\phi_2^{(N-1)}(p) + d_{N-2}\phi_2^{(N-2)}(p) + \ldots + d_1\phi_2'(p) + d_0\phi_2'(p) = 0 \tag{28}$$

respectively, for some constants c_i and d_i, $0 \leq c_i, d_i \leq N$. Note again that the $\phi_1^{(i)}(p)$ and $\phi_2^{(i)}(p)$ are computable from boundary data for any given complex $p \neq 0$, as

$$\phi_j^{(i)} = RG\left(\frac{\partial^i w^j}{\partial p^i}\right).$$

Without loss of generality we may set c_N and d_N to 1. We can then construct a linear system of N equations in the variables c_0 to c_{N-1} or d_0 to d_{N-1} by choosing N different values of p. We then solve this system for the $c_i's$ and $d_i's$. Once we have these coefficients, we then use them in the equations

$$(z^1)^N + \sum_{i=0}^{N} c_i (z^1)^i = 0$$

$$(z^2)^N + \sum_{i=0}^{N} d_i (z^2)^i = 0$$

These are the characteristic equations for ODE's (27) and (28), so solving them gives us the $z_i^1 s$ and $z_i^2 s$ from which we recover the centers (a_i, b_i, c_i) of the voids.

6.2 Determining the Number of Voids

Usually, the number of voids will be unknown, so we will want to determine that first. To do this, we make a guess at the number of voids, say M with $M \geq N$. As before, using M different values of p we form the linear system

$$c_{M-1}\phi^{(M-1)}(p_j) + c_{M-2}\phi^{(M-2)}(p_j) + \ldots + c_1\phi'(p_j) + c_0\phi(p_j) = -\phi^{(M)}(p_j) \qquad (29)$$

for $j = 1..M$, where $\phi = \phi_1$ or ϕ_2.

If we put the system of equations above in matrix format, then the $M \times M$ coefficient matrix will have $\phi^{(M-i)}(p_j)$ as its (i, j) element. If our guess M for the number of voids is the same or greater than the actual number of voids then as shown in [2], the rank of the linear system (29) gives us the number of voids.

However, directly computing the rank of the coefficient matrix will only give the correct number of voids if its elements, $\phi^{(M-i)}(p_j)$, are exact. In most instances, the $\phi^{(M-i)}(p_j)$ will be computed using experimental data. So, while the $\phi^{(M-i)}(p_j)$ may be accurate, depending on the quality of the data, it will rarely be exact.

We estimate the rank of the linear system by performing a singular value decomposition on the coefficient matrix. However, directly computing the rank of the coefficient matrix will only give the correct number of voids if its elements, $\phi^{(M-i)}(p_j)$, are exact. In most instances, the $\phi^{(M-i)}(p_j)$ will be computed using experimental data. We thus perform a thresholding operation to estimate the rank, typically by taking as non-zero only those singular value which exceed some fraction of the largest singular value (usually around 0.01).

6.3 Recovering the Radii

Again, the formula for the radii is similar to that we got in the case of a single void. We state the formula as a theorem:

Theorem 5: Assume there are N spherical voids, each D_i with radius R_i and center

(a_i, b_i, c_i), for $i = 1$ to $i = N$. For any harmonic test function $w = e^{p_x x + p_y y + p_z z}$

$$RG(w_p) = 2\pi \sum_{i=1}^{N} R_i^3 \nabla u_0(a_i, b_i, c_i) \cdot q e^{q \cdot r_i} + O(R^4) \tag{30}$$

where $q =< p_x, p_y, p_z >$ and u_0 is the harmonic function on Ω with Neumann data g

The only difference in the proof is that u is approximated separately near the center of each void. Thus, after similar steps from equations (17) to (22), from page (11), we obtain

$$u_i \approx u_0(a_i, b_i, c_i) + \frac{3}{2} R_i \nabla u_0(a_i, b_i, c_i) \cdot n < \sin\varphi\cos\theta,\ \sin\varphi\sin\theta,\ \cos\varphi > \tag{31}$$

where u_i is the approximation for u in the vicinity of void D_i.

Using (31) in the RG function yields

$$\begin{aligned}
RG(w_p) &= \sum_{i=1}^{N} \int_0^{2\pi} \int_0^{\pi} (u_0(a_i, b_i, c_i) + \frac{3}{2} R_i \nabla u_0(a_i, b_i, c_i) \cdot \mathbf{n})(q \cdot \mathbf{n}) e^{q \cdot r}\ R_i^2 \sin\varphi d\theta d\varphi \\
&= \sum_{i=1}^{N} R_i^2 e^{q \cdot r} \int_0^{2\pi} \int_0^{\pi} u_0(a_i, b_i, c_i)(q \cdot \mathbf{n}) \sin\varphi d\theta d\varphi \\
&+ \sum_{i=1}^{N} \frac{3}{2} R_i^3 e^{q \cdot r} \int_0^{2\pi} \int_0^{\pi} \nabla u_0(a, b, c) \cdot \mathbf{n})(q \cdot \mathbf{n})\ \sin\varphi d\theta d\varphi \\
&= \sum_{i=1}^{N} \frac{3}{2} R_i^3 e^{q \cdot r} \int_0^{2\pi} \int_0^{\pi} \nabla u_0(a_i, b_i, c_i) \cdot \mathbf{n}(q \cdot \mathbf{n})\ \sin\varphi d\theta d\varphi \\
&= \frac{3}{2} \sum_{i=1}^{N} R_i^3 e^{q \cdot r} \cdot \frac{4}{3} \pi \nabla u_0(a_i, b_i, c_i) \cdot q \\
&= 2\pi \sum_{i=1}^{N} R_i^3 \nabla u_0(a_i, b_i, c_i) \cdot q e^{q \cdot r}
\end{aligned}$$

Now that we have Theorem 5 and a means of estimating the center of the voids, we can recover the radii by computing $RG(w_p)$ for N different values of p and then solving the resulting system linear system of equations for the R_i^3, and thus obtain each R_i.

6.4 Numerical Test

Once again we use Femlab to obtain data to test the results above. We use the input heat flux $g = \cos\varphi$ with Ω as the unit sphere with three voids. The p values were taken as 0.2 times the cube roots of unity. The actual void parameters and the recovered values are shown in the table below:

	Actual	Recovered
Centers	(-0.5, -0.3, 0) (0.1, 0.2, 0.7) (0.4, 0.4, -0.3),	(-0.524, -0.344, -0.029) (0.090, 0.197, 0.745) (0.423, 0.423, -0.303)
Radii	0.25 0.20 0.30	0.248 0.210 0.316

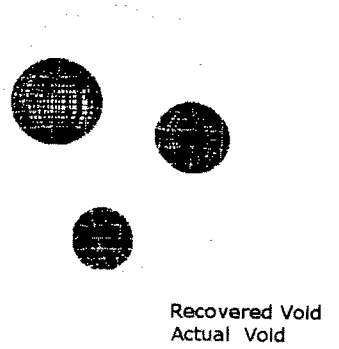

Figure 4: Actual and Recovered Voids

7 Conclusion and Future Work

Thus far, we have successfully developed and implemented an algorithm for accurately recovering spherical voids within an arbitrary domain. The information we get from implementing this algorithm includes the number of voids, their locations, and radii. Our algorithm is based on the reciprocity gap approach, which requires only boundary data for void recovery. This way, our need to test non-destructively is satisfied.

There are several ways this project can be extended. It would be appropriate to see if a different approach can be developed for recovering spherical voids as was done here. A specific direction may be using the Reciprocity gap approach but with a different class of test functions. Another natural extension will be imaging with time with time dependent fluxes. Also, very little work has been done in recovering planar defects in a spherical domain. This will be an appropriate subject for future work.

References

[1] Andrieux, S., and Ben Abda, A., *Identification de fissures planes par une donne de bord unique; un procd direct de localisation et didentification*, C.R. Acad. Sci., Paris I, 1992, 315, pp. 1323-1328.

[2] Bryan, K., Haugh, J., and McCune, D. *Fast Imaging of Partially Conductive Linear Cracks Using Impedance Data*, Inverse Problems 22 (2006), p 1337-1358.

[3] Bryan, K., Rachel Krieger, and Nic Trainor, *Imaging of multiple linear cracks using impedance data*, to appear in J. of Computational and Applied Math.

[4] Bryan, K.,Personal Communication

[5] Brown, D., and Hubenthal, M., *Time dependent thermal imaging of circular inclusions*, Rose-Hulman Mathematics Technical Report 05-01, August 2005.

[6] Talbott, S., and Spring, H., *Thermal imaging of circular inclusions with a two-dimesional region*, Rose-Hulman Mathematics Technical Report 05-01, August 2005.